Welding in the World
https://doi.org/10.1007/s40194-025-02317-7

RESEARCH PAPER

Effect of CW-GMA welding on the HAZ and mechanical properties of structural steel

Victor Igwemezie[1] · Zahraddeen Musa[1] · Supriyo Ganguly[1]

Received: 9 September 2025 / Accepted: 23 December 2025
© Crown 2026

Abstract

This work investigated the effect of cold wire gas metal arc welding (CW-GMAW) on the heat-affected zone (HAZ) and mechanical properties of structural steel designated as BS 970 Part 3:1991 080A15 steel. The study involved feeding cold ER70S-6 wire into the welding arc of energised hot wire (HW). Welds were produced at cold wire feed speeds (CWFS) of 2, 4, and 6 m per min labelled CW2, CW4, and CW6, and were compared with conventional welds (CW0) and the parent metal (PM). Metallographic examination, hardness testing, and cross joint tensile evaluation were carried out. Cold wire (CW) addition resulted in a more gradual cooling profile which increased the width of heat-affected sub-zones particularly the grain refined zone (GRZ). Hardness decreased across all weld zones with increasing CWFS indicating improved ductility and reduced potential for brittle phase formation. Although the 0.2% proof stress reduced by about 16% relative to the parent metal (PM), the tensile strength at CW6 approached that of the base material. Ductility loss of 35% in CW0 reduced to 22% in CW welds representing a 13-point improvement. For CW6, the tensile fracture location shifted from the partially transformed zone (PTZ) to the PM close to PTZ region confirming improved mechanical performance. However, at higher CWFS, weld penetration decreased due to reduced arc energy density. The study demonstrates that CW addition can improve ductility and tensile performance in conventional GMA welds while increasing productivity when welding parameters and joint design are optimised.

Keywords Cold wire gas metal arc welding · Structural steel · Metallography · Hardness · Tensile testing

Abbreviations

%El	Percentage elongation
α	Ferrite
γ	Austenite
CJT	Cross joint test
CGHAZ/CGZ	Coarse grain heat-affected zone
CTWD	Contact tip to workpiece distance
CW	Cold wire
CW-GMAW	Cold wire gas metal arc welding
CW0	Conventional GMAW without addition of external CW
CW2	CW-GMAW with addition of CW at 2 m per minute
CW4	CW-GMAW with addition of CW at 4 m per minute
CW6	CW-GMAW with addition of CW at 6 m per minute
CWFS	Cold wire feed speed
FL	Fusion line
GMAW	Gas metal arc (GMA) welding
GRZ	Grain refined zone
HAZ	Heat-affected zone
HW	Hot wire
HWFS	Hot wire feed speed
PM	Parent material
PS	0.2% Proof stress
PTZ	Partially transformed zone
Q	Heat input
TZ	Tempered zone
UTS	Tensile stress or strength
WFS	Wire feed speed

Recommended for publication by Commission XII - Arc Welding Processes and Production Systems

✉ Victor Igwemezie
victor.igwemezie@cranfield.ac.uk

[1] Welding and Additive Manufacturing Centre (WAMC), Cranfield University, Cranfield, Bedfordshire MK43 0AL, UK

Published online: 17 January 2026

WM	Weld metal
θ	Contact angle

1 Introduction

Heat input (Q) during welding plays a key role in the quality of a welded joint. The energy input is known to significantly affect both the microstructure of the weld metal (WM) and heat-affected zone (HAZ) in the baseplate [1]. High Q is known to promote the formation of coarse grains in the HAZ adjacent to the fusion line [2]. Coarse grains, in turn, promote the development of hard or brittle phases, especially when rapid cooling occurs. These brittle phases reduce the toughness of the coarse grain HAZ (CGHAZ) [3], which affects the overall integrity of the weldment.

A welding process referred to here as cold wire gas metal arc welding (CW-GMAW) has been found to reduce the energy transferred to the base metal during welding and the residual stress developed [4, 5]. This process simply involved the addition of external non-energised cold wire (CW) into the welding arc of energised hot wire (HW) in the GMAW process as illustrated in Fig. 1. In Fig. 1, the CW is fed into the arc created by the HW at a pre-defined angle. The HW feed speed (HWFS) is kept constant, and the CW is added at a specified rate and TS. The CW addition and variation in TS influence the Q.

The aim of this study is to assess the effect of CW addition on the sub-zones of the HAZ and the mechanical properties of BS970 Pt3 1991 080A15 structural steel weld. This information is important in evaluating the industrial applicability of CW-GMAW for the welding and repair of structural steel components. The specific objectives are as follows:

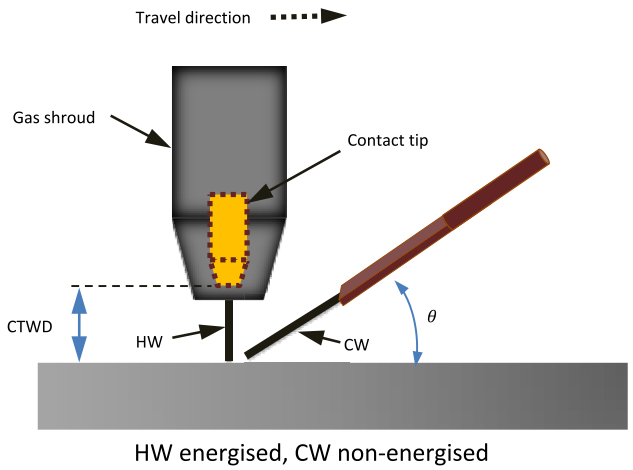

Fig. 1 General CW-GMAW process setup

1. To obtain a process window that provides weld beads with a low contact angle (θ) and reinforcement.
2. To assess the effect of CW addition on the WM and HAZ of the weld joint.
3. To investigate the mechanical properties of the weldment.
4. To compare the mechanical performance of CW-GMA welded joints with those produced by conventional GMAW.
5. To assess the industrial applicability of CW-GMAW based on the results.

To qualify a butt weld in a procedure test, most specifications such as ISO 15614 and ASME IX require a cross joint tensile (CJT) test to be carried out. Hence, CJT was used to assess the weld integrity.

2 Review of recent studies on the CW-GMAW process

In a recent CW-GMAW study by Musa et al. [6], the ER70S-6 electrode was used as the CW and HW in welding S275JR structural steel grade. The CW was fed into the HW welding arc at rates of 0 m/min (CW0), 5 m/min (CW5), and 10 m/min (CW10). The HWFS was fixed at 11 m/min, and the energy inputs were reported as 1.30 kJ/mm for CW0, 1.0 kJ/mm for CW5, and 0.75 kJ/mm for CW10. Figure 2 shows the result of the hardness test performed across the weldment [6].

The graph shows that generally, the addition of CW progressively reduced the hardness level in the weld metal (WM), fusion line (FL), and coarse grain HAZ (CGHAZ) area. The reduction persisted up to about 5 mm from the weld centreline across the CGHAZ (or CGZ) as shown in Fig. 2. In structural steel, under standard arc welding conditions with energy input around 1–2 kJ/mm, the CGZ typically extends up to 1 mm or more from the fusion boundary [2]. Higher energy input can widen the CGZ up to 2 mm. In Fig. 2, therefore, it is reasonable to assert that CW addition reduced the hardness of the CGZ.

This result is important because most weld failures, particularly fatigue failures, start at the weld toe due to the high stress concentration at this point of geometrical discontinuity as illustrated in Fig. 3a [7, 8]. This weld toe commonly lies directly above the CGZ as shown in Fig. 3b [9].

The CGZ often has poor toughness due to the formation of untampered bainitic and martensitic phases [9]. The conditions of the WM and the HAZ are critical to the overall integrity of the weldment. The other zones within the HAZ are noted in Fig. 3b.

In Fig. 2, the hardness reduction of the CGZ extended up to 1 mm from the fusion line. It is expected that the addition

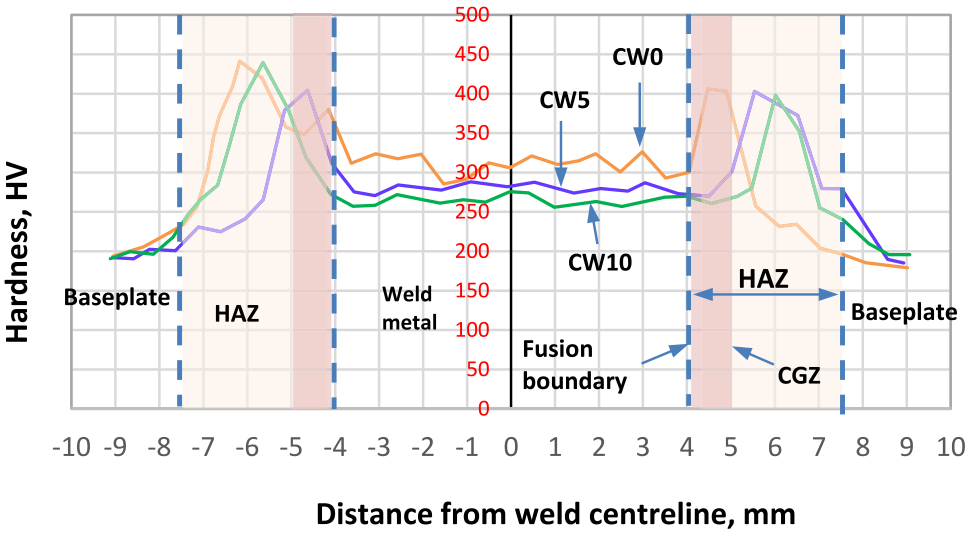

Fig. 2 Hardness profile of CW-GMA welded samples: CW0, CW5, and CW10 [6]

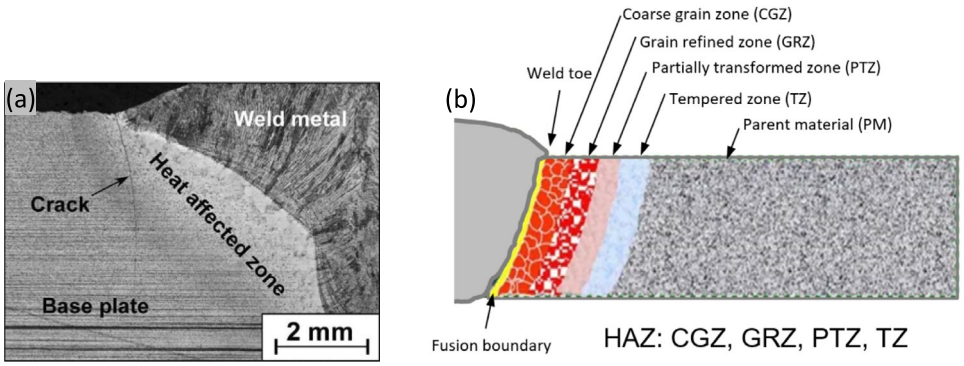

Fig. 3 **a** Joint failure at the weld toe and **b** heat-affected zones

of CW would improve the toughness of the WM and CGZ, which is desirable for the integrity of the welded joint. Musa et al. [6] also reported low penetration with the addition of CW.

Wang et al. [10] studied the behaviour of ER90S-G steel wire used as both HW and CW in the CW-GMAW process. HWFS of 11 m/min was used and the CWFS varied from 0 to 14 m/min. They found that the CW-GMA process reduced the specific energy density, leading to smaller grain sizes and reduced anisotropy. These microstructural changes improved the mechanical properties and minimised anisotropy. They also reported that the addition of CW reduced the remelting of the previously deposited layer and dilution in the fusion area.

Ribeiro et al. [4] studied the feasibility of using CW-GMA process to weld non-heat-treatable aluminium alloy (AA5052 H-32) baseplate with AWS ER5356 wires. They found that the addition of CW reduced porosity more than conventional GMAW. The tensile testing failure was reported to occur outside the HAZ.

Costa Assunção et al. [11] studied the viability of using CW-GMAW to weld a 5-mm-wide groove in 16-mm-thick ASTM A131 Grade A steel plates using ER70S-6 wires. They reported that the welding arc attached to the CW instead of the weld pool, which led to a more stable arc and prevented it from attaching to the groove sidewalls. This helped avoid sidewall grooving. Additionally, fewer passes were required to complete the weld. They observed that the hardness value reduced in the HAZ—particularly for the capping pass. This implies that high carbon structural steel may be welded or repaired without the need for post-weld heat treatment. A similar study [12] using 4-mm-wide narrow gaps machined from API X80 linepipe showed the same result but the decrease in the penetration led to incomplete fusion.

Jorge et al. [13] studied the CW-GMAW process using ASTM 1020 steel baseplate and AWS ER70S-6 wires. They found that the grain size of the CGZ could be reduced and refined, particularly if pulsed CW-GMAW is employed. This was attributed to lower energy input. Also, the CW feeding angle was found to influence this property.

Marques et al. [14] used the ER70S filler wires to weld ASTM A131 Grade A steel using the CW-GMAW. They reported that the addition of CW reduced the amount

of intergranular ferrite, while the hardness of the HAZ increased. The hardness increase is inconsistent with the findings in Refs [6, 11]. They also observed that joints produced with the CW-GMAW exhibited a longer fatigue life, particularly at higher stress amplitudes.

Mohammadijoo et al. [3] investigated the effect of CW addition in tandem submerged arc welding (SAW) of API X70 microalloyed steel plates. Both the HW and CW were 4-mm diameter EA2 electrodes, and the CWFS was initially set at 0.25 m/min. They reported that the CGZ decreased in size, the prior austenite grains (PAGs) were finer, and fewer brittle phases formed. This led to an improvement in the impact fracture toughness of the HAZ. However, when the CWFS was increased to about 0.76 m/min, slender martensite-austenite (M-A) constituents formed due to the relatively faster cooling rate in the CGZ, which negatively affected the toughness.

Generally, CW-GMAW provided a low-energy, microstructural control, toughness improvement, residual stress reduction, arc stability, and bead quality. However, the process requires precise control and risks such as low penetration. Data on the correlation of the CGZ produced as a result of CW addition and the mechanical property of the welded joint appears to be scarce. This gap in knowledge provides part of the motivation for this study.

3 Methodology

This section outlines the experimental procedures used towards achieving the objectives of this study.

3.1 Test Materials

The base material used in this study is a 200 mm by 12 mm steel plate designated in the Mill certificate as BS970 Pt3 1991 080A15 (structural steel). S3NiMo1 (low alloy steel) and 316L (austenitic stainless steel) filler wires were also used for weld bead shape study only. The compositions of the materials are shown in Table 1.

From the composition, 080A15 is a carbon-manganese (C-Mn) steel with trace alloying elements. Due to the increase in Cr and Ni contents, its yield stress (YS) and ultimate tensile strength (UTS) are expected to be high. The plate was used for both the bead-on-plate study and to produce the cross joint test (CJT) samples used in this study. The electrode used for both HW and CW is AWS ER70S-6. It comes in the form of uncoated wire that is widely used for welding structural steels, particularly in MIG/MAG and TIG welding processes. The wire had a diameter of 1.2 mm, and its chemical composition is also listed in Table 1. Weld pool shielding was provided by M20 8% CO_2 in Argon (ISO 14175-M20-ArC-8) at a flow rate of 18 l/min.

3.2 Experimental setup

The CW-GMAW system consists of a KUKA robot, a Fronius Transpulse Synergic 4000 power source, a CW feeding system, an electrical characteristics monitoring system, a welding arc monitoring camera, and a molten metal shielding system. A typical robotic welding setup is illustrated in Fig. 4a.

The whole welding process was automated to ensure consistency and repeatability. Figure 4b is the HW, CW, and angle of inclination of the CW, α. The α was about 43° and contact tip to workpiece distance (CTWD) 17 mm. Figure 4c is a live capture of the welding process.

3.3 Bead shape determination for the CW-GMAW process

Earlier bead on plate studies [10, 13] have found that for high strength low alloy steel (ER90S-G) and ER70S-6 wires, there was a transition from semicircular bead towards elliptical-shaped bead as the CW addition increases in the CW-GMAW process. The point of this transition was not reported. This observation is important because it aids in the selection of the process window for this study. Hence, as an initial study, the bead shape variation with increasing addition of CW was investigated to confirm these studies using the S3NiMo1 and 316L filler wires.

For the first bead shape study, the HW and CW wires were S3NiMo1 wire of 0.9-mm diameter, using shielding gas of 8% CO_2 and 92% Ar and flow rate of 18 l/min. The energy input was kept constant by fixing the HWFS and TS at 21 m/min and 0.6 m/min respectively. The CWFS was then varied from 0 (CW0) to 8 (CW8) m/min. The effect on the bead shape is shown in Fig. 5.

It was found that the bead height increased gradually with the addition of CW, while the bead width remained

Table 1 Chemical composition of test materials

Grade	C	Mn	Si	Cr	Ni	Mo	Sn	Al	N	P	S
080A15	0.17	0.75	0.20	0.17	0.14	0.03	0.03	0.001	0.01	0.01	0.03
ER70S-6	0.08	1.46	0.85	-	-	-	-	-	-	-	-
S3NiMo1	0.11–0.14	1.30–1.60	0.10–0.20	≤0.1	0.9–1.00	0.5–0.60	-	≤0.04	-	≤0.008	≤0.008
316L	0.01	1.80	0.40	18.3	11.7	2.6	-	-	-	-	-

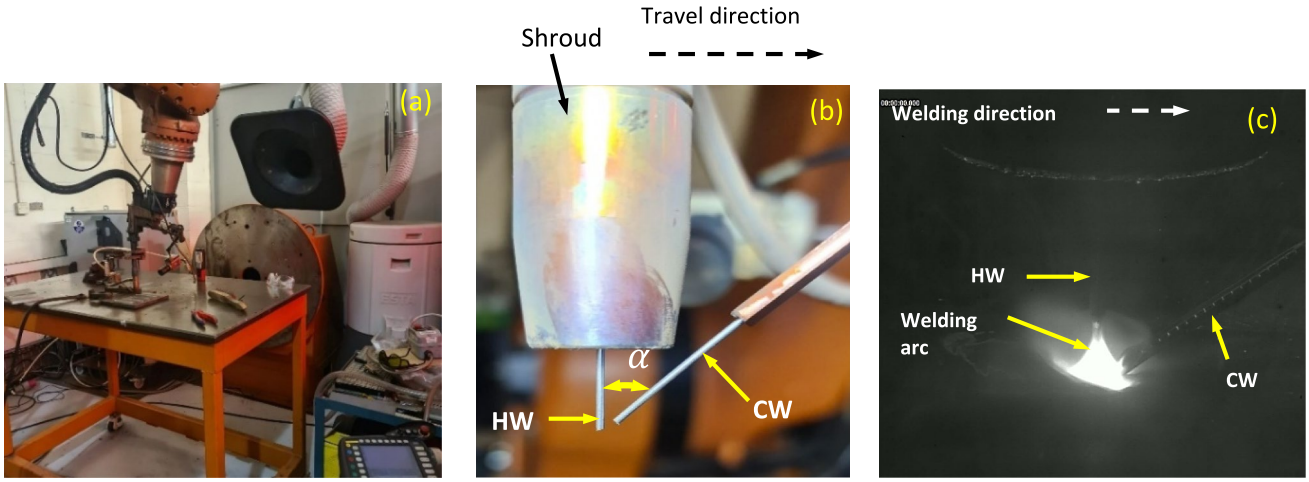

Fig. 4 **a** Robotic welding setup. **b** HW and CW feeding setup. **c** CW-GMAW live process

Fig. 5 Bead cross-sections showing effects of CW addition for ER80S-Ni1 wire

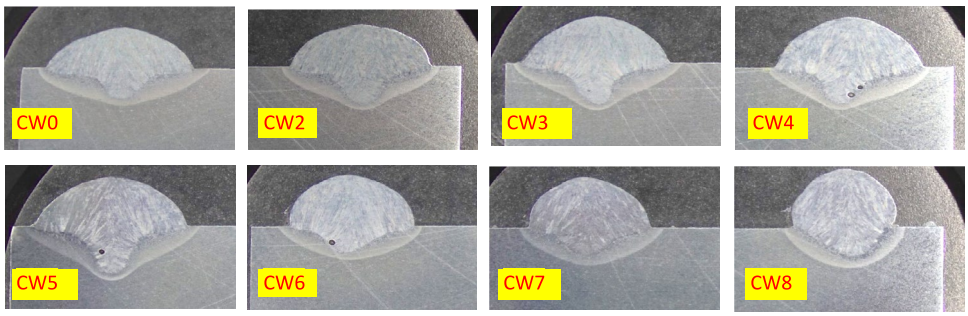

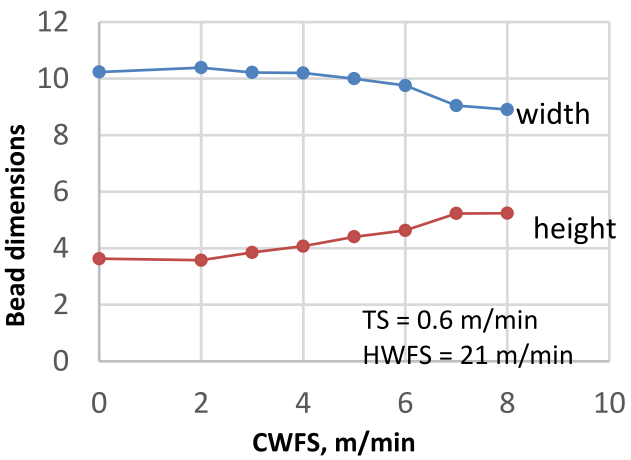

Fig. 6 Effect of increase in CWFS on bead dimensions at fixed energy input

generally constant but noticeably decreased beyond a CWFS of 6 m/min as shown in Fig. 6. Additionally, the bead shape transitioned from semicircular to elliptical as can be seen in Fig. 5.

In the second bead shape study, 316L wire of 1.2-mm diameter was used as the HW and CW. The intention was to understand the effect of increased alloying elements on the bead dimension and transition point in the additive welding. The 316L is a high alloy content wire compared to ER70S-6, ER90S-G, and S3NiMo1. The energy input was kept constant by fixing the HWFS and TS at 12 m/min and 0.6 m/min respectively. The CWFS was from 0 to 15 m/min as noted in Fig. 7.

Considering the results in Fig. 5 and Fig. 7, it can be asserted that increasing CW addition leads to a transition from a semicircular to an elliptical bead shape, typically starting at about CWFS of 6 m/min. However, the exact point of this transition appears to be influenced by the alloying elements in the wire. The transition tends to set in earlier with increasing alloying element content.

It has been observed that an elliptical bead promotes slag entrapment, which in turn causes lack of fusion along the fusion line and is therefore undesirable. Consequently, to achieve a quality weld using CW-GMAW, the bead should remain semicircular. Based on this observation, the maximum CWFS of 6 m/min was selected for this study.

3.4 Process study for HW parameters

To add CW, a suitable and stable HW needs to be established for the ER70S-6 wire that is to be used for 080A15

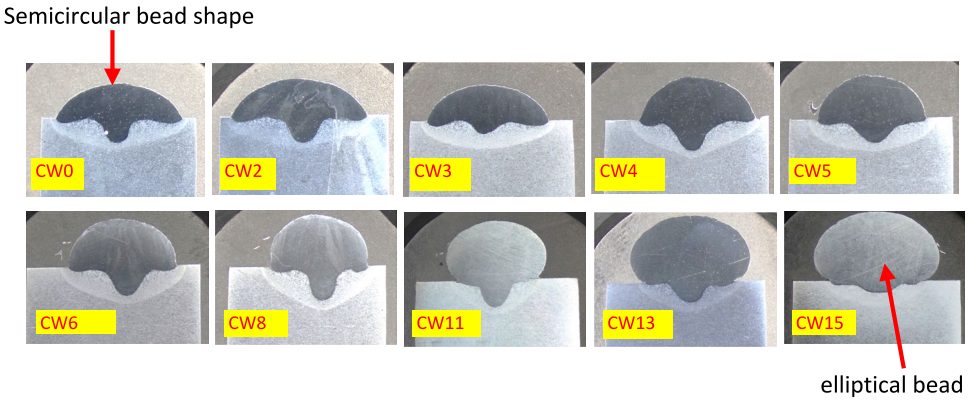

Fig. 7 Effect of increase in CWFS on bead shape for 316L

Fig. 8 Bead-on-plate for process selection using S355 baseplate

steel welding. Hence, a bead-on-plate technique as shown in Fig. 8 was employed. Before deposition, the substrates were cleaned using a wire brush and acetone.

The HWFS was selected to operate in the spray metal transfer mode in the range 10 to 13 m/min, and TS in the range of 0.2 to 1.9 m/min. A bead-on-plate of 100 mm in length was then made on 080A15 baseplate. Three readings were taken at the start, middle, and end areas of the bead length and the average values of the width and height were plotted against the TS. The Q (or energy per unit length) was also plotted against TS. The Q was calculated using the following formula [15]:

$$Q = \frac{0.8 * U * I}{1000 * \mathrm{TS}_{(\mathrm{mm/s})}} (\text{in kJ/mm}) \quad (1)$$

where 0.8 = thermal efficiency of MIG/MAG welding process, TS in mm/s (m/min*16.67 = mm/s).

Figure 9 shows the data trend for the Q vs. TS and bead dimensions vs. TS. It was observed that the tendency to produce defective or irregular beads increased from TS of 1.0 m/min for all HWFS as indicated in the coloured box. Above 2.0 kJ/mm, the Q was considered to be high in this study.

It can be seen that the TS controls the Q and the bead dimensions. A decrease in TS increased the Q (Fig. 9a), the bead width (Fig. 9b) and height (Fig. 9c). To select a desired weld profile, an optimal combination of the three parameters needs to be considered. However, it was observed that a HWFS of 12 m/min, marked in Fig. 9d, and a CTWD of 17 mm produced a very stable, long arc that facilitated the addition of CW, with little or no spatter. This parameter was then selected for the CW-GMAW study. The average voltage at HWFS of 12 m/min was 39 V, and the current of 305 A. These parameters were measured using the AMV 5000 instrument.

3.5 Process study for CW addition

The next task was to determine the effect of the addition of the CW on the stability of the arc produced by the HWFS at 12 m/min. The study has shown that the transition from a semicircular to an elliptical bead for ER70S-6 shape begins at about CWFS of 6 m/min. Therefore, the process window for this study was limited to CWFS values between 0 and 6 m/min. Other factors that affected the CW-GMAW were the CW feeding angle (θ), CTWD, and the arc length correction (AC). These factors were varied independently until a good, uniform bead and little or no spatter were obtained for the CWFS range of 0 to 6 m/min.

Figure 10a shows the bead on plate for the addition of the CW and Fig. 10b is the result of the process study with the addition of CW from 0 to 6 m/min for TS of 0.5, 0.6, 0.9, and 1.2 m/min—denoted as 0.5TS, 0.6TS, 0.9TS, and 1.2TS respectively. Figure 10b shows that the bead dimensions decreased with an increase in the TS. The figure also shows that the bead height increased gradually with the addition of the CW. However, the bead heights of 0.5TS and 0.6TS aligned. This tends to show that TS below 0.6TS affects only the bead width and not the height.

An important note is that for each TS, the bead width remains relatively constant as the CW increased from 0 to 6 m/min, and this helps in comparative analysis of the

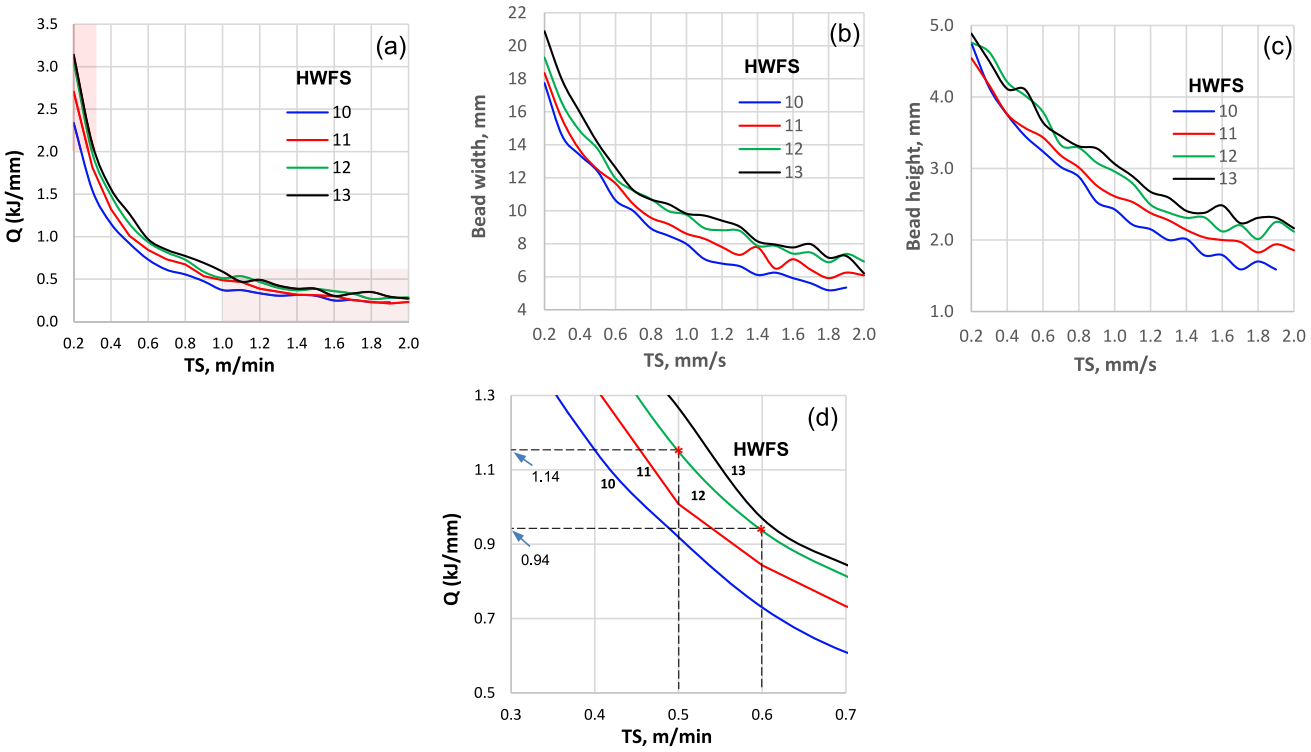

Fig. 9 The effect of TS on the EPUL and weld bead dimensions

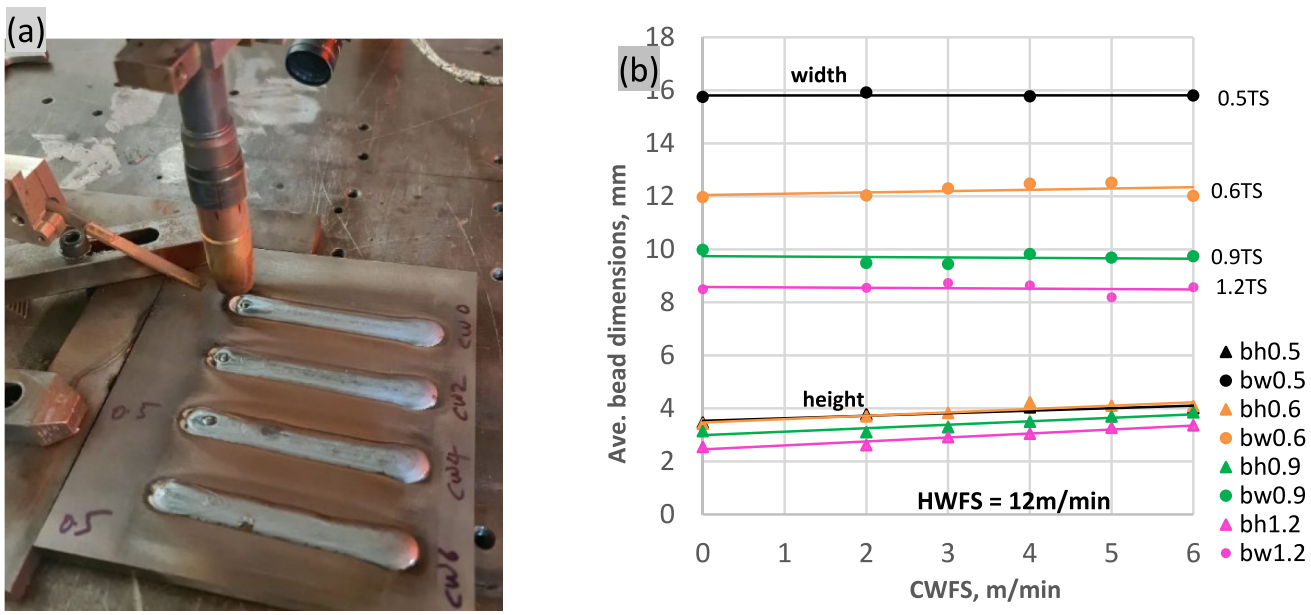

Fig. 10 **a** The bead-on-plate of CW addition; **b** the effect of addition of CW on the bead dimensions

joint filling characteristics of the CW addition. Within the whole range, the CW-GMAW process maintained a stable arc and produced a consistent bead quality.

Figure 11 shows a bead-on-plate for 0.5TS and 0.6TS, showing bead uniformity and stable process. A suitable TS, sufficient to ensure effective melting of the baseplate, is desirable. The TS should maintain the weld arc ahead of the molten weld pool to allow direct heating of the baseplate.

For the CJT test piece production, TS of 0.5 and 0.6 m/min, with Q values of 1.14 and 0.94 kJ/mm respectively (as

indicated in Fig. 9d), was selected for trials due to their bead uniformity and stable CW-GMAW process. Note that lower TS was not desired to avoid excessive Q to the weld joint and to maintain the welding arc ahead of the weld pool.

3.6 Test material preparation

To select the final parameters for the CJT test, the parameters in Table 2 were tried on a grooved baseplate shown schematically in Fig. 12a. CW0, CW2, CW4, and CW6 represent CWFS of 0, 2, 4, and 6 m/min respectively. Two weld passes were used, and no grinding of previous weld was performed. The first layer was brushed clean before the deposition of the second layer. Figure 12b shows the comparison of the filling characteristics of CW2 and CW4 for 0.5 and 0.6TS. It was observed that 0.5TS had better groove filling characteristics across the three CWFSs. The welded plate was then sectioned and examined for defects. It was again observed that 0.5TS produced a better quality weld.

The final parameters HWFS 12 m/min and TS 0.5 m/min were then used to weld the baseplate shown schematically in Fig. 13a. There was consistency in the start and finish points during the welding. Figure 13b is the welding and welded samples from which the tensile samples were extracted. During welding, the test piece was held rigidly to prevent distortion. Two weld passes were used to fill the joint.

In Fig. 13, narrow butt joint welding was employed to reduce the volume of molten metal required to fill the joint. This approach helps minimise residual stresses and distortion. The joint configuration helps to promote heat flow into the baseplate in a transverse direction or to achieve two-dimensional heat-flow conditions, rather than radially or three-dimensional heat flow, as is typically the case with a V-butt joint. Additionally, the second pass to fill the joint would not significantly alter the HAZ from the initial pass, as the second bead would essentially be deposited on top of the first. The configuration would also help to assess the defect tendencies of the CW-GMAW.

Table 2 Parameters used for test sample preparation

Parameter	Value
HWFS	12 m/min
U_{ave}	39 V
I_{ave}	305 A
CW feeding angle	43°
CTWD	17 mm
Travel speeds (TS)	0.5 m/min, 0.6 m/min
CWFS (for each TS)	0, 2, 4, 6 m/min

3.7 Metallography and hardness survey

Standard metallography procedures (ISO 17639 [16]) were used to characterise the microstructure of the weldment, particularly the WM and HAZ. Polishing was performed using a mechanical polisher with a 3-µm diamond suspension, followed by etching with 2% Nital for 3 to 4 s. All macro-sections were examined, measured, and hardness tested using standard laboratory equipment equipped with digital imaging and analysis software. The average hardness across the weldment was evaluated using standard Vickers hardness testing (HV10), applying a 10 kg load with a dwell time of 10 s in accordance with ISO 9015-1 [17], ISO 6507-1 [18]. And root and sidewall penetrations were also assessed. Figure 14 shows the measurement scheme employed in the hardness survey. The indentations were taken at 2 mm below the surface of the PM and the spacing was 1 mm.

3.8 Tensile test specimen

Figure 15a shows the dimensions of the CJT specimens used in this study with Gauge length = 50 ± 0.1 mm. This dimension was chosen to enable comparison with vast tensile data in the public domain. The dog-bones were extracted from the welded plates shown in Fig. 13b and from the area bounded by the red lines in Fig. 14. For statistical control, three samples were prepared for each welding condition—CW0, CW2,

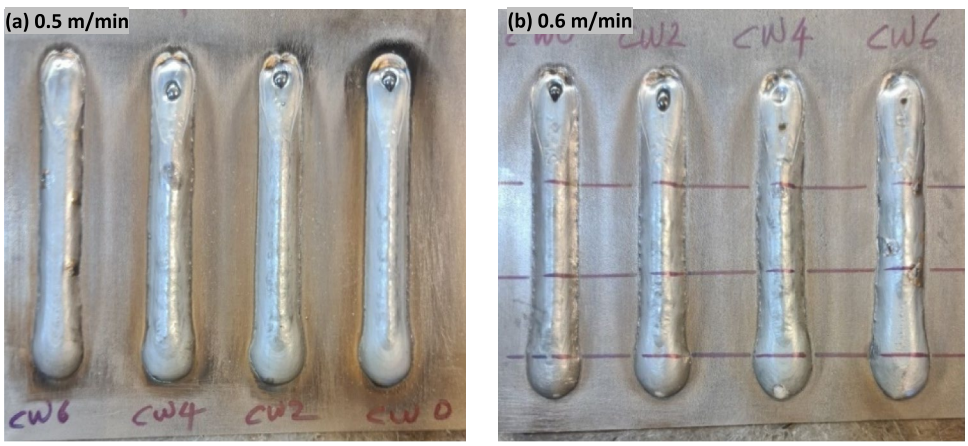

Fig. 11 Bead-on-plate for TS of **a** 0.5 m/min and **b** 0.6 m/min for the CW-GMAW process

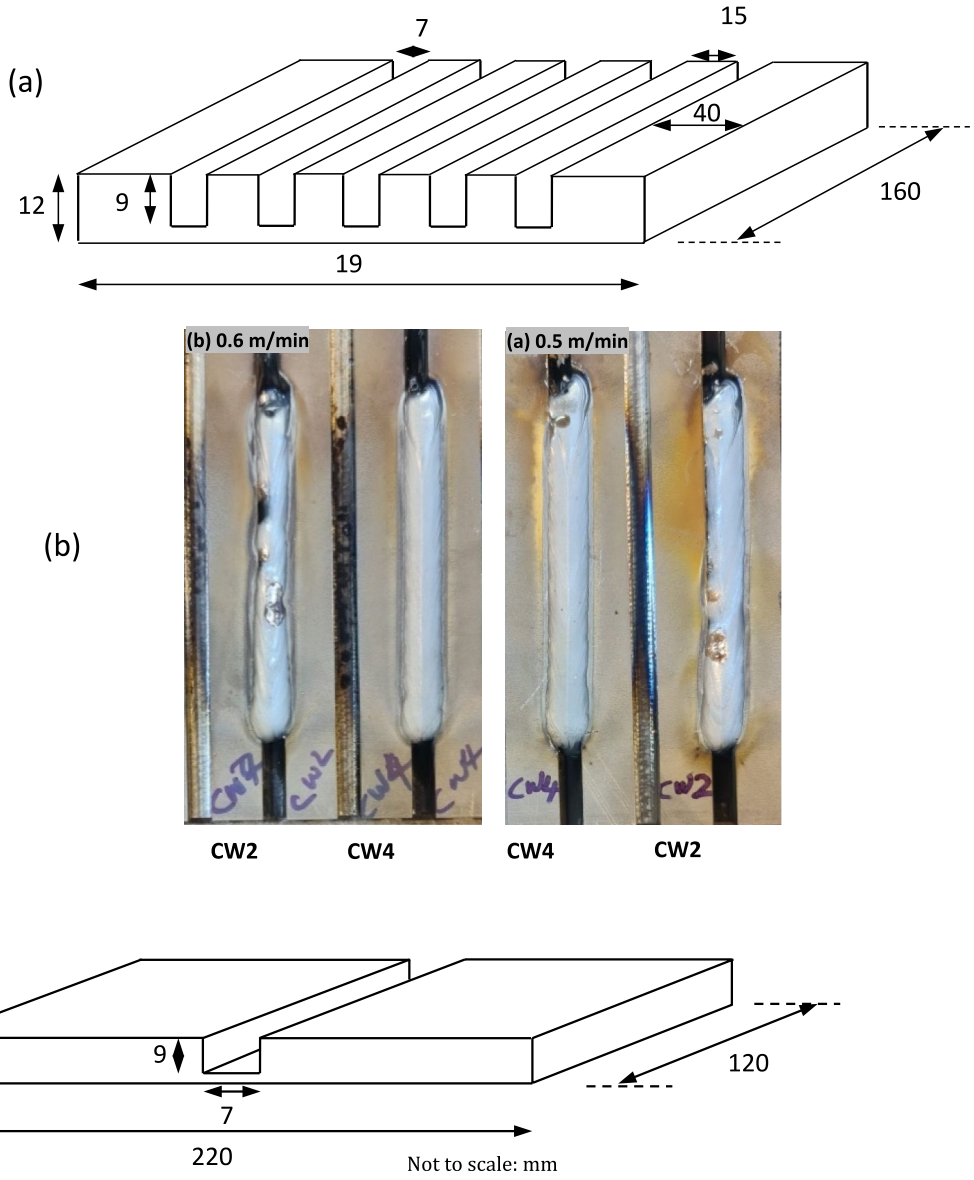

Fig. 12 **a** Grooved baseplate for trial welds; **b** groove filling trial for TS of 0.5 and 0.6 m/min

Fig. 13 **a** Schematic of butt joint; **b** welded plates for tensile samples' extraction

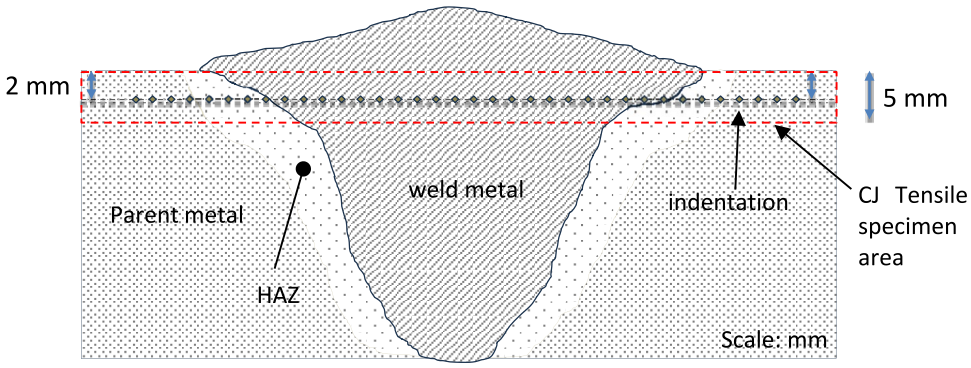

Fig. 14 Location of the indentations in hardness survey

CW4, CW6, and CS (control sample). Figure 15b shows the extracted test specimens, and the testing was conducted in accordance with ASTM E8/E8M – 15a [19]. Figure 15c shows the Instron 68 FM-100 testing machine with a laser extensometer used for testing of all the samples.

4 Experimental results and discussion

The effects of CW addition at 2, 4, and 6 m/min on weld quality, compared with the conventional weld (CW0) and PM, have been evaluated using metallography, hardness, and tensile testing. This section presents the results obtained in this study and the discussions on the results.

4.1 Metallographic survey

Figure 16 shows the macrographs of the welded sections of CW0, CW2, CW4, and CW6. The welds showed complete fusion and no defects within the tensile sample extraction area highlighted by the yellow box on CW0 in Fig. 16. The same area applies to CW2, CW4, and CW6. Figure 17a shows the microstructure of the weldments, which typically

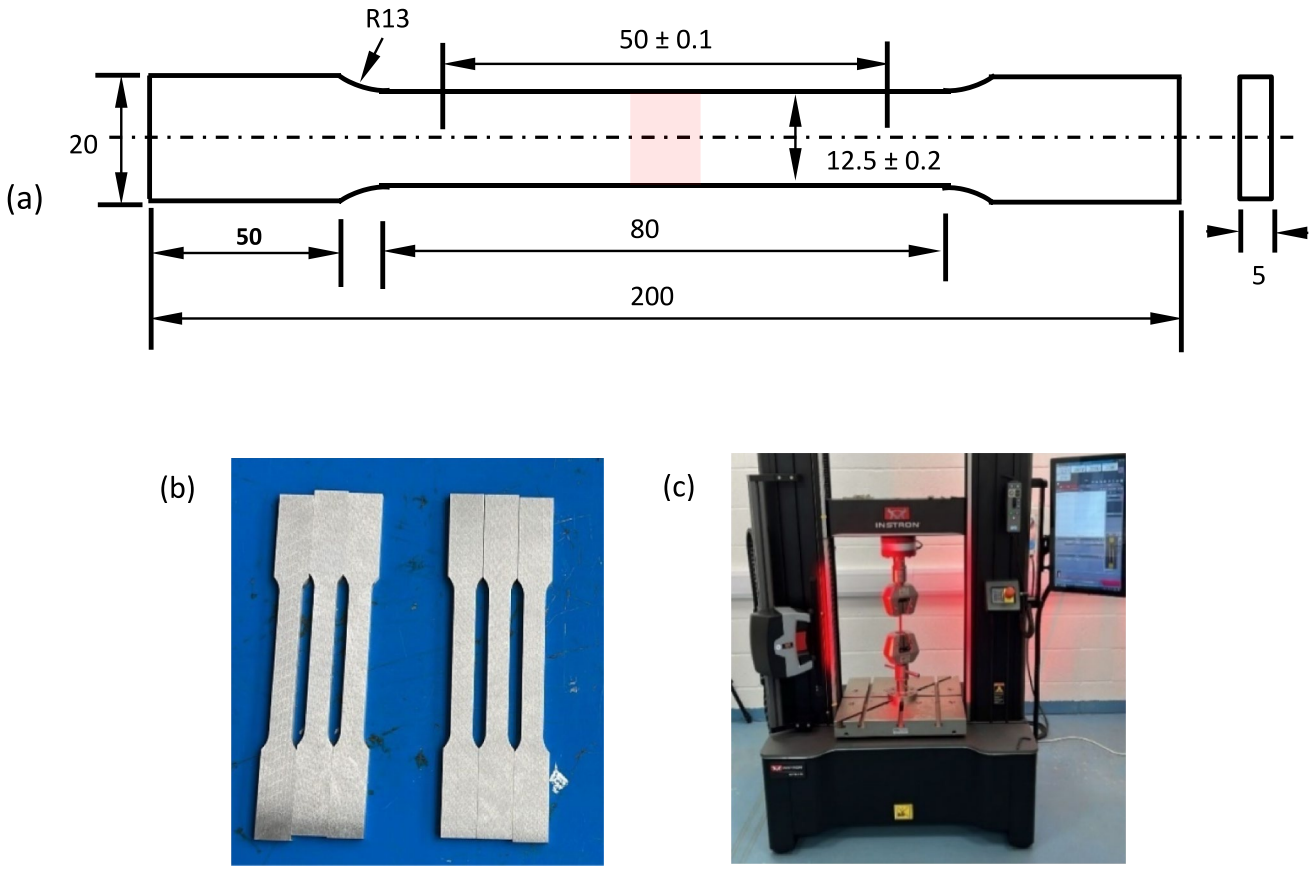

Fig. 15 Rectangular tension test specimens

consists of the WM and the HAZ. Figure 17b–e shows the sub-regions within the HAZ of the weldment. Figure 17b is the weld metal (WM), Fig. 17c is the coarse grain zone (CGZ), Fig. 17d is the grain refined zone (GRZ), Fig. 17e is the partially transformed zone (PTZ), and Fig. 17f is the parent metal (PM). The tempered zone (TZ) is also present but could not be distinguished from the PM. Apart from variation in the width of the sub-regions in the HAZ, a similar microstructure was obtained for all the weld samples.

To characterise the HAZ, the width of each sub-region within the HAZ was measured as shown in Fig. 18. The 4 samples were cut at exact positions in the middle of the weld length. To quantify the width, a horizontal reference line was drawn passing through the weld toe. The corresponding micrographs were then imported into image analysis software, and measurements were conducted based on the embedded scale. The scale bar on the micrograph was first calibrated to a known length (200 units), establishing a consistent measurement basis. Subsequently, the distances between specific points were estimated: the span from point 1 to point 2 was used to determine the width of the CGZ; point 2 to point 3 corresponded to the GRZ; and point 3 to point 4 is that of PTZ, as illustrated using the micrograph of sample CW0 in Fig. 18. The width of the TZ was not quantified, as the boundaries of this region cannot be virtually defined due to the absence of observable microstructural transformations.

Figure 19 shows the measured microstructures of CW0, CW2, CW4, and CW6 welds and the results of these measurements (in microns, μm) in Fig. 19 are plotted in Fig. 20.

From the plot, a slight increase in the widths of both the CGZ and the PTZ is observed. However, a substantial increase in the GRZ is evident, with the increment reaching at least 157 μm compared to CW0. In other words, the percentage increase from CW0 to CW6 is approximately 36%. It is clear that all the three sub-regions of the HAZ expanded in width with the addition of CW. Therefore, it can be asserted that CW addition leads to a corresponding increase in the size of the HAZ sub-regions.

The microstructural evolution across the HAZ, as usual, varied with peak temperatures experienced during the welding. In the GRZ, peak temperature was insufficient to cause grain growth, resulting in fine microstructures with potentially superior mechanical properties compared to the CGZ [20].

The thermal profile across the weld is governed by the balance between Q and conduction. The addition of CW in this study resulted in less intense heating and a more gradual thermal gradient. In other words, a slower change in temperature over distance was obtained. This leads to a more uniform heat distribution and, consequently, a wider HAZ, particularly in the GRZ as seen in Fig. 20.

4.2 Hardness survey

Vickers hardness measurements were taken 2 mm below the surface, with a spacing of 1 mm between indentations, as shown in Fig. 21. A 10 kg load was applied for 10 s in accordance with ISO 9015–1 [17]. Figure 22 presents examples of indentations in the PM, PTZ, GRZ, and CGZ and

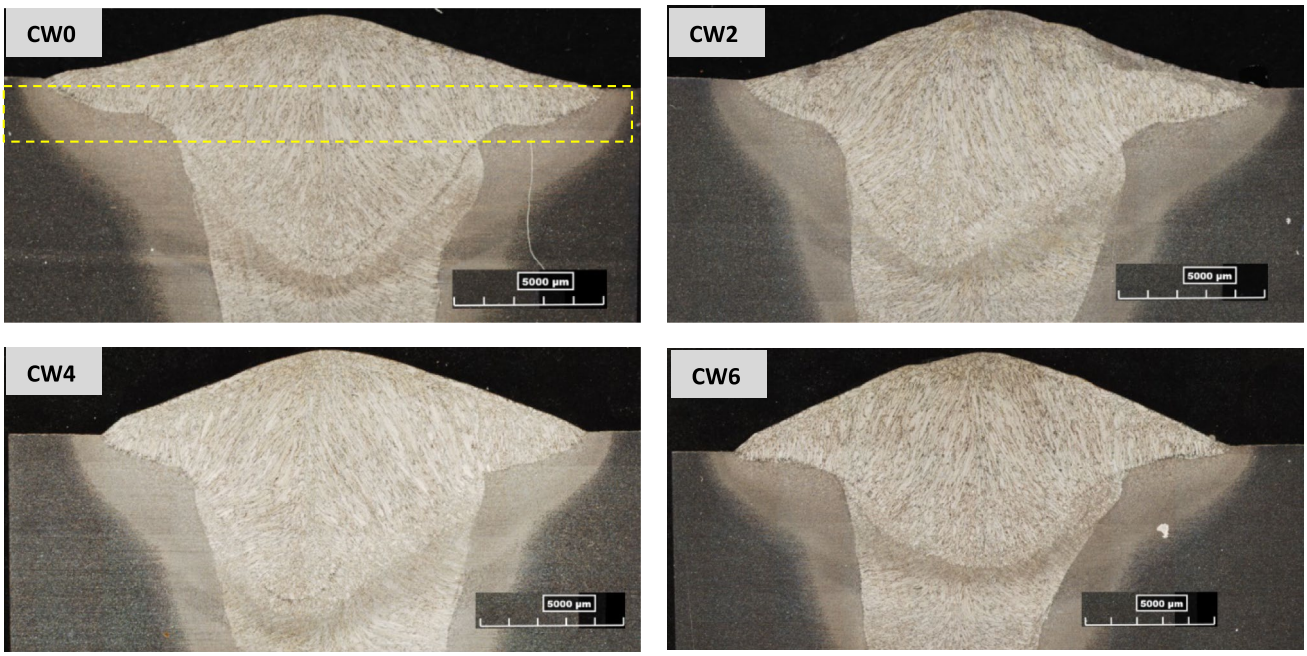

Fig. 16 Typical macrographs of the welded test plates

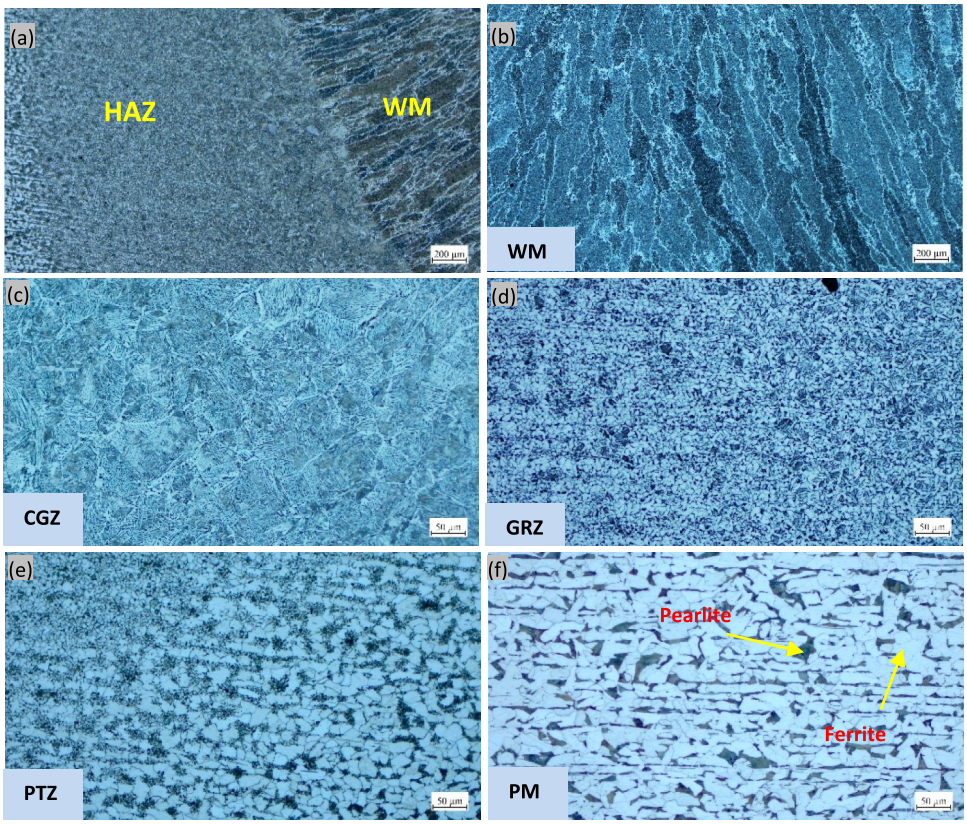

Fig. 17 Microstructures of the weldment and sub-regions within the HAZ of BS970 Pt3 1991 080A15 steel (HWFS = 12 m/min, TS = 0.5 m/min, U = 39 V, I = 305 A)

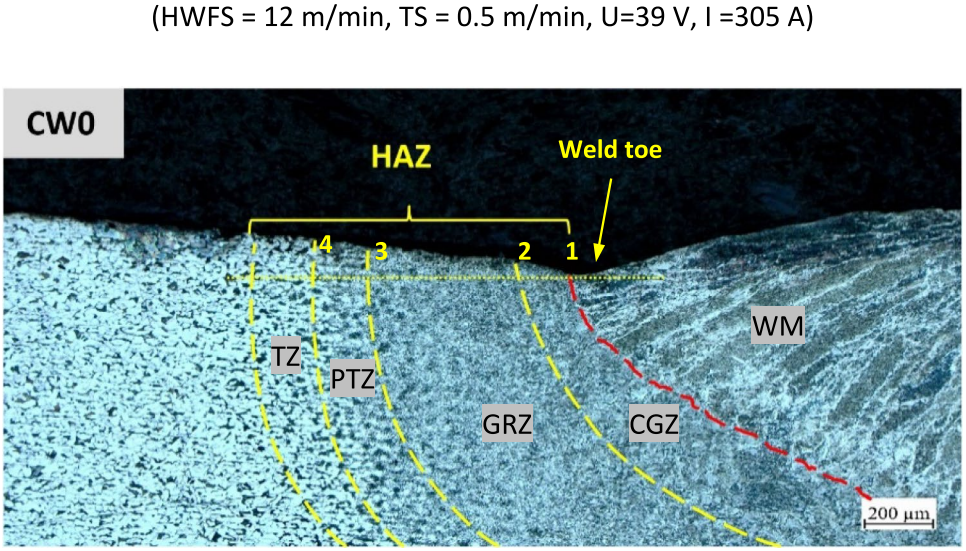

Fig. 18 Method for the measurement of width of the sub-regions of HAZ

regions of the CW6 samples. The average HV10 values across the HAZ and WM for all test samples are plotted in Fig. 23. The average hardness of the PM, based on 20 data points, is 201 HV.

As shown in Fig. 23, hardness generally decreased with increasing CW addition across all weld zones. For CW2 and CW4, CGZ hardness was nearly equal to WM, while in CW6, CGZ dropped below PM. In other words, WM and CGZ showed the highest hardness at lower CW levels (CW0–CW4), but at CW6, PM hardness exceeded the WM and all the HAZ sub-regions. Across all CW-added samples, GRZ and PTZ consistently showed the lowest hardness values, falling below that of the PM. Hardness is generally lowest in PTZ.

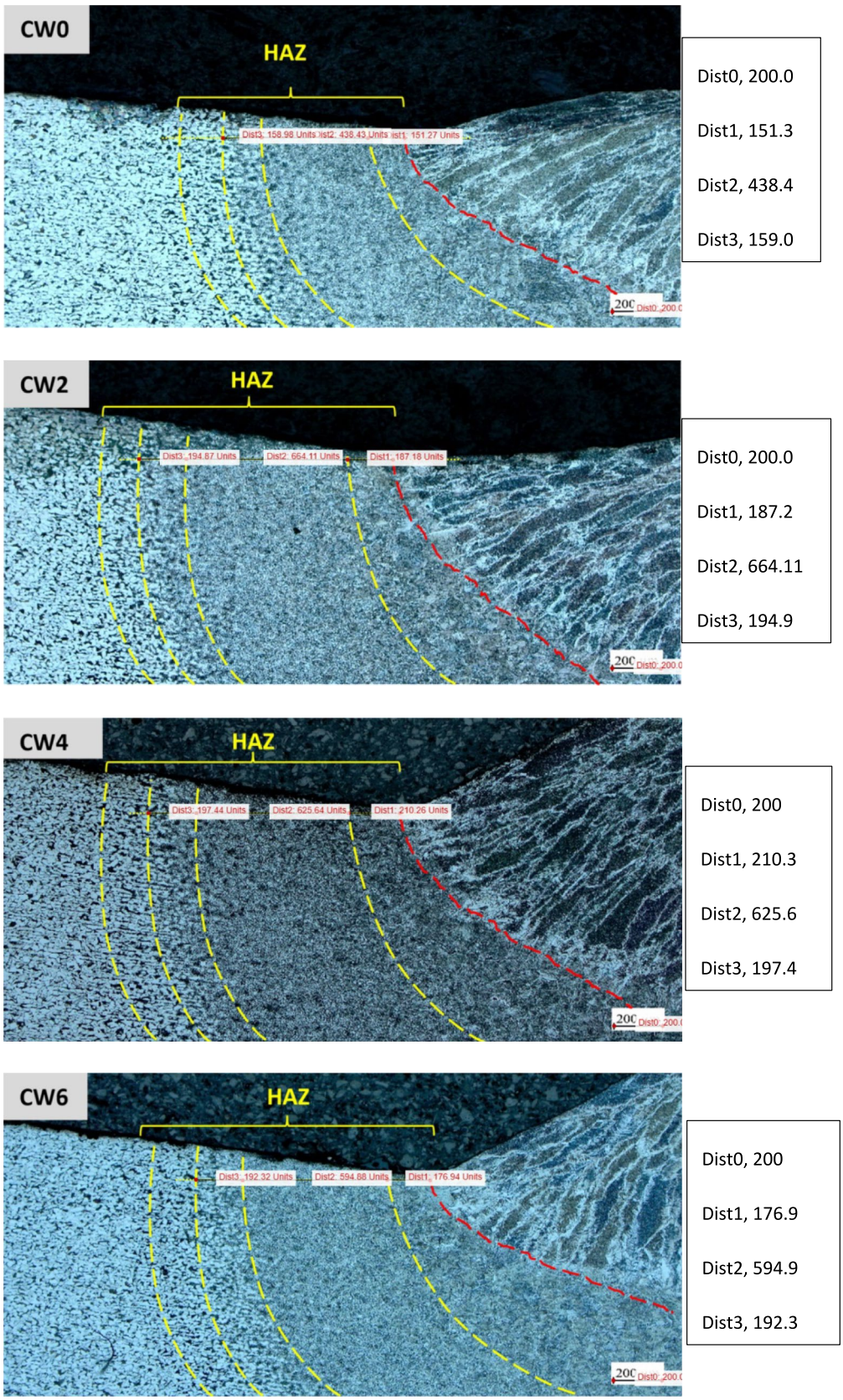

Fig. 19 Microstructures of CW0, CW2, CW4, and CW6 welds

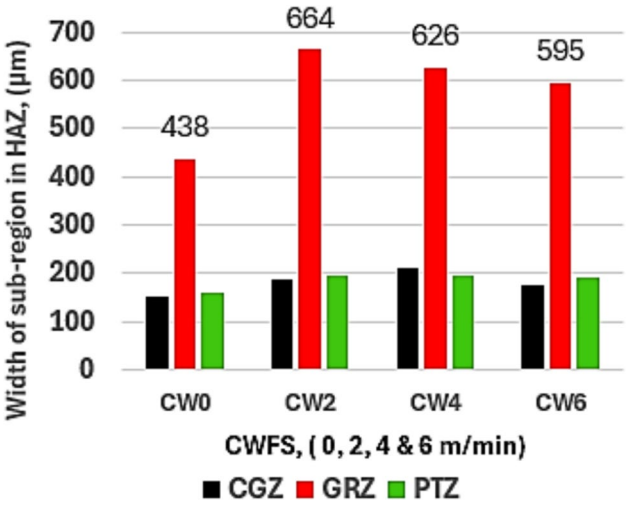

Fig. 20 Plots of CGZ, GRZ, and PTZ width dimensions

These results indicate that CW addition reduced the formation of hard phases across the weldment, suggesting a potential improvement in ductility compared to conventional weld. However, the consistent decrease in hardness within the PTZ across all CW samples, with values significantly lower than the PM, implies the dominance of soft ferrite. This softening, while beneficial for ductility, may coexist with some brittle microstructural constituents that could act as sites for stress concentration, crack initiation, and reduced toughness.

4.3 Tensile test results

The CJT specimen consists of six distinct zones: WM, CGZ, GRZ, PTZ, TZ, and PM. These zones have different mechanical properties, which can make the measurement of the 0.2% proof stress (PS) and percentage elongation (%El) inaccurate and unreliable. However, these parameters were still assessed to understand how they compared to CW0. The key properties investigated in this test include the PS, UTS, %El, and the location of fracture.

Figure 24a shows the plotted graphs of PS, UTS, and %El results. The control sample (CS) is the mechanical properties of the PM. The graph clearly shows that the PS and ductility of the CW samples are lower than that of the CS. However, the UTS of the CW samples improved and approached that of the CS in sample CW6. Also, the conventional weld CW0 has the lowest ductility and UTS. This trend is clearly presented in Fig. 24b and c.

Figure 24b shows a reduction in PS from 549 MPa in the CS to 482 MPa in the CW0. With the addition of CW, PS further decreased to 464 MPa in sample CW2, a value that remained roughly consistent in CW4 and CW6. The average PS across all CW samples is about 463 MPa, indicating that CW addition did not significantly alter PS; however, the value is lower than both values of PM and CW0. A similar trend was observed in TS. The TS decreased from 611 MPa in the CS to 598 MPa in CW0. Subsequent addition of CW increased the TS from CW0 to CW6. In fact, the TS of sample CW6 approached that of the baseplate, suggesting that CW addition can enhance TS of the weldment. Figure 24c shows a clear reduction in ductility from approximately 23% in the PM to 15% in the CW0. However, the addition of CW significantly improved the ductility compared to CW0. The average ductility recorded across all CW samples was 18.2%.

The ductility loss in CW0 compared to baseplate can be stated thus

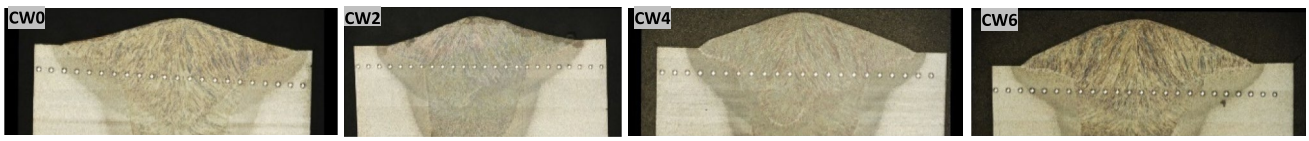

Fig. 21 Hardness measurements method

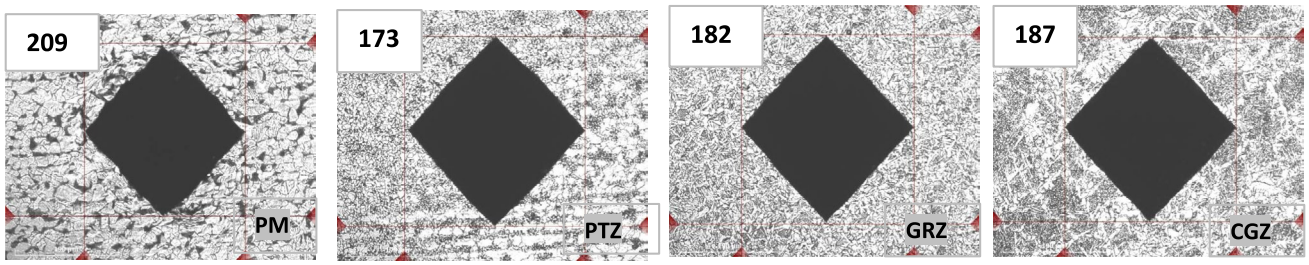

Fig. 22 Hardness indentations at different sub-regions within HAZ

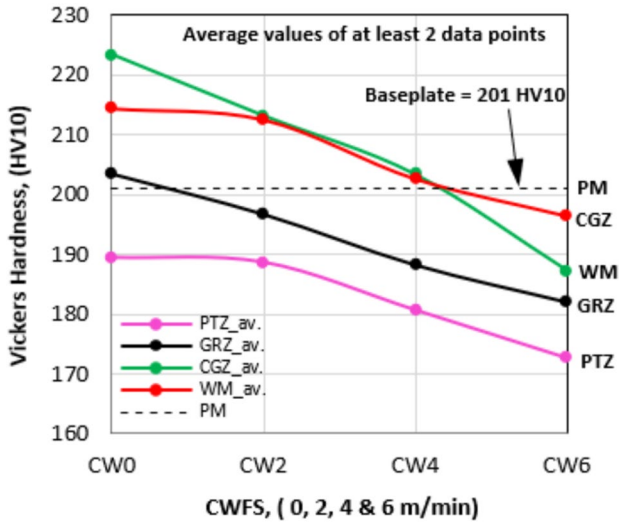

Fig. 23 The plot of hardness survey data

$$\text{Percentage loss} = \frac{23-15}{23} \times 100 \cong 35\% \quad (2)$$

Ductility loss in CW-added samples compared to baseplate:

$$\text{Percentage loss} = \frac{23-18}{23} \times 100 \cong 22\% \quad (3)$$

Recovery as a percentage of the original loss (from CW0):

a. Conventional loss = 8
b. CW-added loss = 5

$$\text{Recovery } \% = \frac{8-3}{8} \times 100 \cong 38\% \quad (4)$$

Thus, the CW-added samples recovered approximately 38% of the ductility that was lost in the conventional weld. This means that CW addition significantly improved ductility performance over conventional welding without the use of preheat or post-weld heat treatment.

4.3.1 Position of fracture

For conventional welding, the WM commonly has higher strength than the PM, so failure generally occurs in the parent. The location of failure is of interest in this study as it defines the weakest point in the weldment under static loading. Figure 25 shows the failure locations for the samples. The CS represents the failure scenario of the baseplate. In sample CW0, failure initiated in the PTZ. In samples CW2 and CW4, failure occurred either in the PTZ or in the region between the PTZ and the PM. Failures in the PTZ suggest the presence of detrimental brittle phases in this area, making it the weakest link in the weldment.

In sample CW6, failure is observed in the PM, but close to the PTZ. This indicates that the weldment in CW6 can have tensile properties close to the PM, although its ductility is reduced from 23% in the parent to 18%, representing about a 22% reduction. However, without preheating or post-weld heat treatment, CW-added samples recovered about 38% of the ductility that was lost in the CW0. The reason why the strength of CW6 approached that of PM, with failure occurring in the PM close to the PTZ, might be attributed to factors, such as the broader zone of refined grain size in the HAZ (see Fig. 17), and tempering of the coarse grain region caused by the shallow temperature gradient introduced by the CW addition. Note that the refined grains are smaller than those of the PM. These two factors can increase the toughness of the weld zone. Fracture is not expected in the WM because of the presence of acicular ferrite which offers very high toughness.

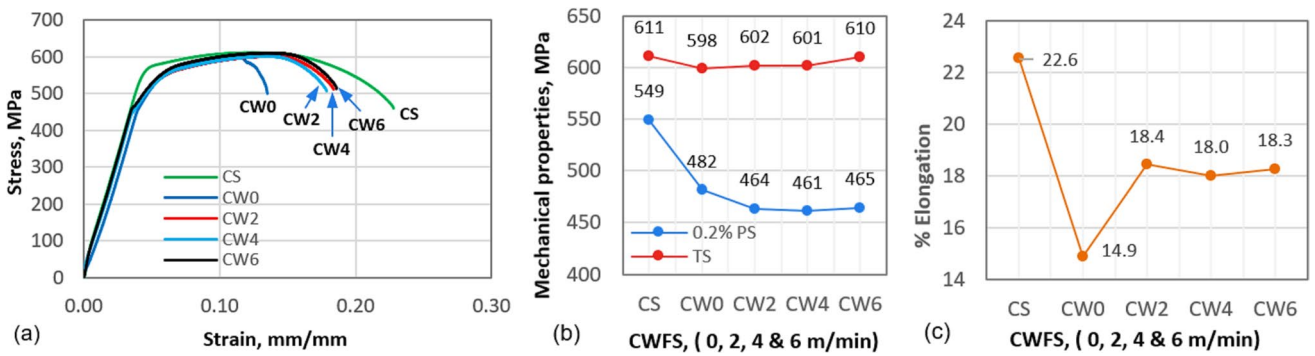

Fig. 24 The plots of mechanical properties of CS, CW0, CW2, CW4, and CW6

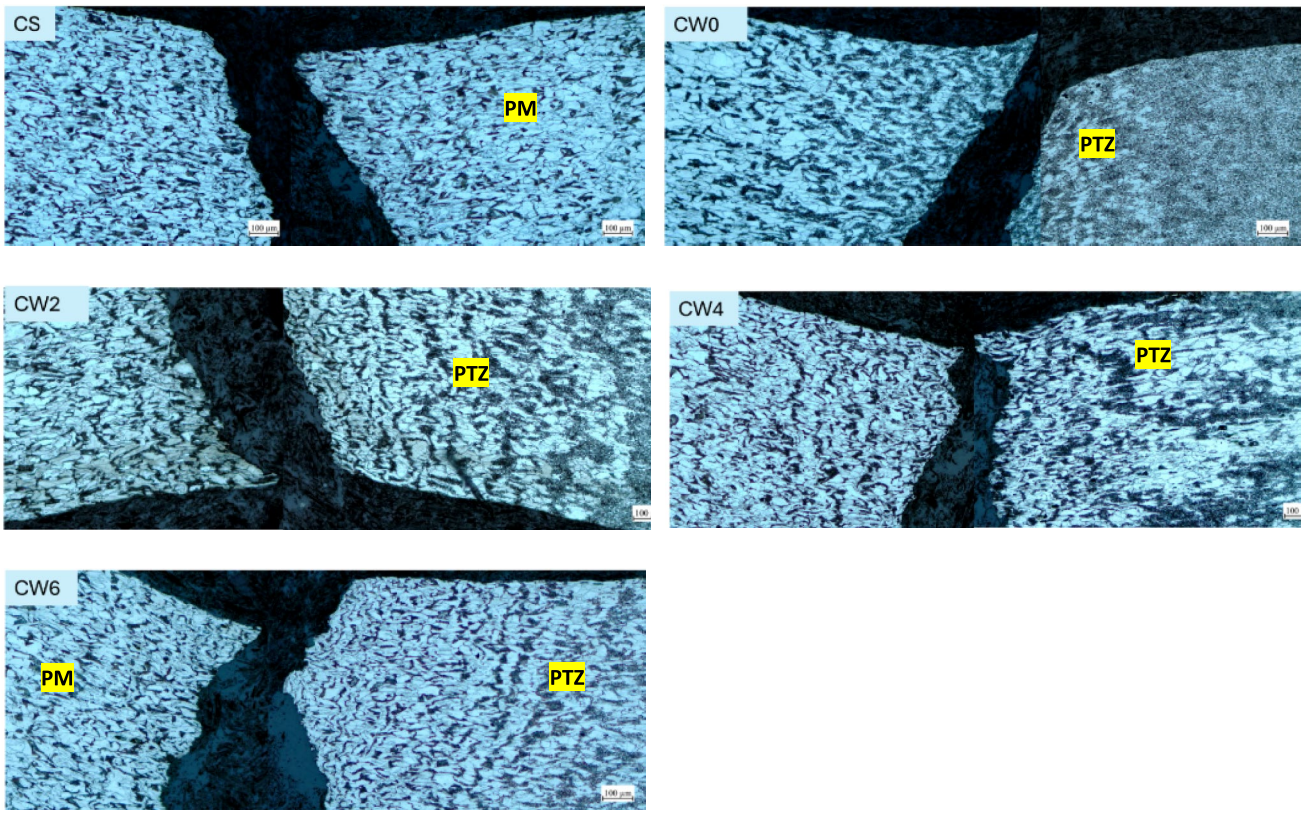

Fig. 25 Position of fracture during tensile testing

Table 3 Comparison of SAW and CW-GMAW

Process	HWFS m/min	CWFS m/min	TS m/min	Wire dia. mm	DR kg/hr	MPUL kg/m	V	I	Q kJ/mm
GMAW (CW0)	12	0	0.5	1.2	6.4	0.21	39	305	1.14
CW-GMAW (CW4)	12	4	0.5	1.2	8.5	0.28	39	305	1.14
CW-GMAW (CW6)	12	6	0.5	1.2	9.6	0.32	39	305	1.14

5 Comparison of GMAW and CW-GMAW productivity

If deposition rate (DR) is given as

$$\mathrm{DR} = \rho\pi r^2(\mathrm{HWFS} + \mathrm{CWFS})\left[\text{in kg/h}\right] \tag{5}$$

The material per unit length (MPUL) becomes

$$\mathrm{MPUL} = \frac{\mathrm{DR(kg/h)}}{\mathrm{TS_{m/h}}}\left[(\mathrm{kg/m}) \text{ or } (\mathrm{g/mm})\right] \tag{6}$$

where density $(\rho) = 7860$ kg/m^3 and $\pi = 3.142$. Table 3 shows that the DR for GMAW would be about 6.4 kg/h and the MPUL 0.21 kg/m. The values for CW4 and CW6 are 8.5 kg/h and 9.6 kg/h, and 0.28 kg/m and 0.32 kg/m respectively. This shows that the CW6 has 50% higher DR and about 52% higher MPUL than CW0. Thus, additive weld can have better joint property and productivity as high as 1.5 times that of conventional weld.

6 Conclusion

The CW-GMAW process is a high-productivity welding technique with the potential to produce exceptional weld quality due to its ability to reduce thermal gradients. In this study, its influence on the HAZ and on the mechanical properties of structural steel designated as BS 970 Part 3:1991 080A15 was evaluated with the aim of applying the process to medium thickness constructions. The investigation examined the effect of cold wire additions at feed rates of 2, 4, and 6 m/min on weld quality, and compared the results with those from conventional welding and

with the properties of the base plate. The welded joints were evaluated using metallographic analysis, hardness measurements, and tensile testing. The study found that

1. Cold wire addition led to increased widths of all subzones within the HAZ, particularly the GRZ which is generally associated with more favourable mechanical properties compared to the CGZ.
2. Hardness values decreased consistently across all weld zones with increasing CW addition. This reduction, particularly in the CGZ, suggests an overall improved weld ductility, which is associated with toughness.
3. 0.2% PS reduced with addition of CW by about 16% from the baseplate. However, UTS generally improved with CW additions, and at 6 m/min achieving a value close to the baseplate.
4. Compared to the baseplate, ductility dropped by 35% in the conventional weld (CW0), while the CW-added samples showed a reduced loss of 22% which represents a 37% recovery in ductility loss in CW0.
5. Failure occurred in the PTZ for CW0 to CW4, confirming it as the weakest zone. For CW6, the fracture location is in the PM close to the PTZ indicating improved mechanical properties of the weld zone, though ductility remained about 22% reduced from the base metal.
6. The addition of CW expanded all HAZ sub-regions, especially the GRZ, indicating a broader thermal influence. However, mechanical test results show no negative impact on weld quality as compared to CW0.

Author contribution Conceptualisation, design, material preparation, investigation, data collection, analysis, original draft preparation, and editing were performed by Victor Igwemezie. Zahraddeen Musa assisted in data collection and experimentation. Supriyo Ganguly reviewed, edited, and supervised the work. All authors read and approved the manuscript.

Funding No funding was received for conducting this study.

Data availability All data for this work have been included in this study. Raw data are available on request.

Declarations

Competing interests The authors declare no competing interests.

Open Access This article is licensed under a Creative Commons Attribution 4.0 International License, which permits use, sharing, adaptation, distribution and reproduction in any medium or format, as long as you give appropriate credit to the original author(s) and the source, provide a link to the Creative Commons licence, and indicate if changes were made. The images or other third party material in this article are included in the article's Creative Commons licence, unless indicated otherwise in a credit line to the material. If material is not included in the article's Creative Commons licence and your intended use is not permitted by statutory regulation or exceeds the permitted use, you will need to obtain permission directly from the copyright holder. To view a copy of this licence, visit http://creativecommons.org/licenses/by/4.0/.

References

1. Bhadeshia HKDH, Honeycombe RWK (2017) Steels microstructure and properties, 4th ed. Elsevier Ltd
2. Shome M (2007) Effect of heat-input on austenite grain size in the heat-affected zone of HSLA-100 steel. Mater Sci Eng A 445:454–460. https://doi.org/10.1016/j.msea.2006.09.085
3. Mohammadijoo M, Kenny S, Collins L, Henein H, Ivey DG (2017) Characterization of haz of API X70 microalloyed steel welded by cold-wire tandem submerged arc welding. Metall Mater Trans A Phys Metall Mater Sci 48:2247–2259. https://doi.org/10.1007/s11661-017-4041-x
4. Ribeiro RA, Assunção PDC, Sengupta V, Khan R, Gerlich AP (2023) Feasibility of cold wire gas metal arc welding AA5052 H-32. J Manuf Process 101:53–66. https://doi.org/10.1016/j.jmapro.2023.05.092
5. Costa ES, Assunção PDC, Dos Santos EBF, Feio LG, Bittencourt MSQ, Braga EM (2017) Residual stresses in cold-wire gas metal arc welding. Sci Technol Weld Join 22:706–713. https://doi.org/10.1080/13621718.2017.1306014
6. Musa Z, Ganguly S, Suder W, Igwemezie V, Rajamudili K. Impact of cold-wire gas metal arc welding (CW-GMAW) parameters on microstructure and microhardness characteristics in repairing S275JR structural steel. TMS 2025 154th Annu. Meet. Exhib. Suppl. Proceedings. TMS 2025. Miner. Met. Mater. Soc., Springer; 2025, p. 1352–63.
7. Schork B, Kucharczyk P, Madia M, Zerbst U, Hensel J, Bernhard J et al (2018) The effect of the local and global weld geometry as well as material defects on crack initiation and fatigue strength. Eng Fract Mech 198:103–122. https://doi.org/10.1016/j.engfracmech.2017.07.001
8. Zerbst U (2020) Application of fracture mechanics to welds with crack origin at the weld toe—a review. Part 2: welding residual stresses. Residual and total life assessment. Weld World 64:151–169. https://doi.org/10.1007/s40194-019-00816-y
9. Zerbst U (2019) Application of fracture mechanics to welds with crack origin at the weld toe: a review Part 1: consequences of inhomogeneous microstructure for materials testing and failure assessment. Weld World 63:1715–1732. https://doi.org/10.1007/s40194-019-00801-5
10. Wang C, Wang J, Bento J, Ding J, Pardal G, Chen G et al (2023) A novel cold wire gas metal arc (CW-GMA) process for high productivity additive manufacturing. Addit Manuf 73:1–15. https://doi.org/10.1016/j.addma.2023.103681
11. Costa Assunção PD, Ribeiro RA, Emanuel EB, Gerlich AP, de Magalhães Braga E (2017) Feasibility of narrow gap welding using the cold-wire gas metal arc welding (CW-GMAW) process. Weld World 61:659–666. https://doi.org/10.1007/s40194-017-0466-5
12. Ribeiro RA, Assunção PDC, Dos Santos EBF, Filho AAC, Braga EM, Gerlich AP (2019) Application of cold wire gas metal arc welding for narrow gap welding (NGW) of high strength low alloy steel. Materials Basel. https://doi.org/10.3390/ma12030335
13. Jorge VL, Scotti FM, Reis RP, Scotti A (2020) The effect of pulsed cold-wire feeding on the performance of spray GMAW. Int

J Adv Manuf Technol 107:3485–3498. https://doi.org/10.1007/s00170-020-05247-4
14. Marques LFN, Santos EBF, Gerlich AP, Braga EM (2017) Fatigue life assessment of weld joints manufactured by GMAW and CW-GMAW processes. Sci Technol Weld Join 22:87–96. https://doi.org/10.1080/13621718.2016.1194735
15. BSI. BS EN 1011–1:2009 - Welding. Recommendations for welding of metallic materials. General guidance for arc welding – BSI British Standards 2009.
16. BSI. ISO 17639:2003 Destructive tests on welds in metallic materials — macroscopic and microscopic examination of welds 2003.
17. BSI. BS EN ISO 9015–2:2016: Destructive tests on welds in metallic materials - hardness testing - part 2: microhardness testing of welded joints 2016.
18. BSI. BS EN ISO 6507–1-Metallic materials. Vickers hardness test. Part 1: Test method 2023.
19. ASTM E8. ASTM E8/E8M-15a Standard test methods for tension testing of metallic materials. ASTM Stand 2015:1–27. https://doi.org/10.1520/E0008.
20. Bhadeshia HKDH, Honeycombe RWK (2017) Steels: microstructure and properties. Elsevier

Publisher's Note Springer Nature remains neutral with regard to jurisdictional claims in published maps and institutional affiliations.

https://dspace.org/

Effect of CW-GMA welding on the HAZ and mechanical properties of structural steel

Igwemezie, Victor; Musa, Zahraddeen; Ganguly, Supriyo

2026-12-31
Springer
https://doi.org/10.1007/s40194-025-02317-7
Igwemezie V, Musa Z, Ganguly S. (2026) Effect of CW-GMA welding on the HAZ and mechanical properties of structural steel. Welding in the World, Available online 17 January 2026

Downloaded from a DSpace repository. https://dspace.org/